Full Length Article

Ullmann coupling of 2,7-dibromopyrene on Au(1 1 1) assisted by surface adatoms

Jinbang Hu[a,b,c], Jinping Hu[a,b], Zhengde Zhang[a,b], Kongchao Shen[a,d], Zhaofeng Liang[a], Huan Zhang[a,b], Qiwei Tian[e], Peng Wang[f], Zheng Jiang[a,b,g], Han Huang[e], Justin W. Wells[c], Fei Song[a,b,g,*]

[a] Key Laboratory of Interfacial Physics and Technology and Shanghai Institute of Applied Physics, Chinese Academy of Sciences, Shanghai 201204, China
[b] University of Chinese Academy Sciences, 101000 Beijing, China
[c] Center for Quantum Spintronics, Department of Physics, Norwegian University of Science and Technology, Trondheim NO-7491, Norway
[d] Department of Physics, Zhejiang University, Hangzhou 310027, China
[e] School of Physics and Electronics, Central South University, Changsha 410012, China
[f] Department of Applied Physics, College of Electronic and Information Engineering, Shandong University of Science and Technology, Qingdao 266590, China
[g] Shanghai Synchrotron Radiation Facility, Zhangjiang Laboratory, Shanghai Advanced Research Institute, Chinese Academy of Sciences, Shanghai 201210, China

ABSTRACT

Ullmann coupling on coinage metals has attracted significant attention in surface chemistry due to its atomic precision of constructing extended covalent nanostructures with predictability, while the elementary reaction mechanism behind has not been comprehensively understood yet. In this study, we demonstrate the active contribution of surface atoms in promoting Ullmann coupling of 2,7-dibromopyrene (Br_2Py) on Au(1 1 1) accompanied with the structure transformation from self-assembly to covalently bound one-dimension polymer chains via a combination of scanning tunnelling microscopy (STM), X-ray photoelectron spectroscopy (XPS) and density functional theory calculations (DFT). Even the organometallic intermediate on Au substrate has been occasionally reported before, it is interesting herein to observe organometallic intermediates with the gold-carbon bonding, and demonstrate that surface adatoms specially play an important role in the dehalogenation process of Br_2Py on Au(1 1 1) as elucidated by DFT simulations. Step-wise annealing facilitates the decoupling of the coordinated Au atoms from organometallic oligomers and the ultimate formation of extended polymers, which has been consistently interpreted by XPS and DFT calculations. Our study might shed new insights on the atomistic understanding of Ullmann coupling chemistry on Au substrates and proposes an effective approach to comprehensively elucidate the effect of organometallic intermediates towards on-surface Ullmann coupling reaction.

1. Introduction

Bottom-up fabrication of stable organic architectures linked by covalent bonds as demanded has drawn tremendous interest over the past decades [1–3], driven by their appealing application potential in both fundamental science and industrial fields, such as nanoelectronics and sensing devices [4,5]. Under this context, a collection of covalent coupling reactions has been extensively explored inspired from the traditional bulk chemistry, including homocoupling of alkynes and various dehalogenative coupling [6–10]. Especially, the dehalogenated aryl-aryl coupling of selected precursors in the presence of coinage metal atoms under UHV conditions, also known as surface-assisted

Ullmann coupling, has been witnessed as an effective and controllable approach to link precursors into oligomers, polymer chains towards building high-stability covalent nanostructures at the single atom level [11–19]. Generally speaking, on-surface Ullmann polymerization comprises several crucial steps: a) the dehalogenation of precursors and the formation of reactive residue intermediates, b) the formation of an organometallic (OM) intermediate on surfaces or the reactant can also be anchored to the metal surface after dehalogenation and no OM structures can be formed, and c) the removal of the coordinated metal atom for the C−C bond formation between monomers Despite the encouraging achievement of on-surface Ullmann reaction, there still exist obvious hurdles which prevent the vast application of the constructed

conjugated nanostructures, for instance, restricted structure quality with limited length of one- dimensional (1D) chains or considerable defects embedded in two-dimensional (2D) network with limited size, mostly due to the fact that the governing mechanism of Ullmann coupling reaction on surface has not been comprehensively understood yet. For instance, several intrinsic limitations are always discovered during Ullmann coupling reaction, the irreversible reaction with locked defects frustrating the formation of extended domains and the surface fouling of detached halogen atoms blocking further polymerization on surface [20]. Importantly, control of the reaction pathway with atomistic understanding of elementary reaction steps is crucial for precise fabrication of covalent nanostructures. For example, the possibility to have competing reaction pathways is observed with molecular degradation in combination with polymerization [21,22], while the template effect and self-assembly strategy have also been proven to significantly influence reaction pathways and the on-surface Ullman coupling afterwards [23–25].

Aiming at the achievement of highly ordered and defect-free covalent nanostructures through C−C bonding, deep insight into the reaction mechanisms and kinetics of on-surface Ullmann coupling process becomes especially crucial [26–29]. Specifically, the reaction inevitably leads to the formation of OM phases, which can be difficult under some circumstances to thermally transform into covalently bonded nanostructures without desorbing or damaging molecules. While in some other cases, unexpected OM intermediates can also be formed showing the mechanism complexity of on-surface synthesis [30]. Interestingly, the formation of OM phases on Au substrates has been seldom observed while carbon-metal-carbon bonds are commonly discovered on Ag surface in Ullmann coupling, which is interfered by the thermodynamic behaviour of Ullmann coupling on Au(1 1 1) with reversible debromination and surface-stabilized residues [28]. On the other hand, the demonstration of the occasional formation of Au coordinated OM chains [22,31–34] indicates that surface adatoms or defects on Au (1 1 1) surface can be the active site to initiate the scission of carbonhalogen bonding under certain conditions and promote the subsequent formation of carbon-metal bonding. In addition, Au itself possesses remarkable activity with special chemical nature and has been widely investigated in catalyst, surface science and so on. With this consideration, the fundamental exploration of the evolution of OM intermediates during Ullmann coupling reaction on Au(1 1 1) would gain invaluable insight onto the reaction mechanism [35], and promote the atomistic understanding of the elementary reaction which is essential to fully elucidate on-surface Ullmann coupling process towards significantly improving the structure quality of polymerized nanostructures.

Herein, the self-assembly and dehalogenation of 2, 7-dibromopyrene (Br_2Py) [36] on Au(1 1 1) at elevated temperatures have been thoroughly investigated by a combination of scanning tunnelling microscopy (STM), X-ray photoelectron spectroscopy (XPS) and density functional theory (DFT) calculations. While experimental results demonstrate the formation of OM intermediates during Ullmann coupling reaction, the Au adatom on surface is expected to have important contribution to the dehalogenation process, which acts as the coordination site as revealed from DFT simulations. Furthermore, converting of OM structures into covalent polymerized chains is straightforward by thermal annealing and kicking out the coordinated Au atom. With the elementary reaction pathway being clarified, to some extent, our findings demonstrate that surface adatoms might play a significant role in promoting the on-surface Ullmann coupling reaction on Au (1 1 1) and the ultimate formation of extended 1D polymers.

2. Experimental methods and DFT calculations

All STM measurements are performed in an ultrahigh vacuum (UHV) system (Omicron Fermi SPM) with the base pressure better than 2×10^{-10} mbar at liquid nitrogen temperature. The sample is grounded while the bias voltage is applied to the tip. STM images were recorded in a constant-current mode. Moderate filtering (for example, smooth and background subtraction) has been applied to STM images for better illustration. A clean and structurally well-defined Au(1 1 1) surface was achieved by cycles of bombardment with Ar + ions and subsequent annealing at 800 K, while the surface quality was double checked by XPS and STM. Commercially available Br_2Py (Richest Group) was thoroughly degassed several hours before deposition inside a glass crucible. The sublimation of Br_2Py was performed with the Au (1 1 1) substrate kept at RT and the deposition rate was monitored by a quartz microbalance. XPS measurements were performed in a separate UHV chamber utilizing the PHIBOS 100 analyzer (SPECS) equipped with a monochromatic Al-Ka radiation (hv = 1486.6 eV), and the base pressure is better than 5×10^{-10} mbar [37]. The photon energy was calibrated against the Au $4f_{7/2}$ core level and the metal Fermi level.

Calculations were performed using the Vienna ab initio simulation Package (VASP) under the framework of DFT [38]. The PBE functional [39] was used in combination with the third-generation van der Waals dispersion correction due to Grimme (DFT-D3) [40,41] and the projector-augmented wave (PAW) ansatz for the atomic cores. A plane-wave cut-off energy of 500 eV was employed, while the k-point sampling was chosen to be $3 \times 3 \times 2$ in order to obtain a realistic and accurate picture of the energetics. For simulation of the OM intermediate with Au−C bonding and the C−C coupled dimer, a three-layer atomic slab of Au(1 1 1) supercell (7×8) with lateral dimension of 20.16×23.04 Å and a two-layer slab of Au(1 1 1) supercell with lateral size 37.44×34.56 Å were utilized, respectively. A vacuum layer of 19 Å was introduced to isolate the interactions of slabs from each other. The lattice parameter of the Au(1 1 1) surface after optimization was found to be 2.88 Å. The top most Au(1 1 1) layer was free together with the adsorbed molecule during geometry optimization, while the bottom two Au(1 1 1) layers were kept fixed. Geometries were optimized until the forces on the active atoms dropped below 0.02 eV/Å. The convergence criterion is 10^{-4} eV in total energy difference. Transition states were predicted using the climbing-image modified nudged elastic band theory (CI-NEB) [42].

3. Results and discussion

When deposited onto Au(1 1 1) at room temperature (RT) with the total coverage of around one monolayer (ML), Br_2Py molecules immediately self-assemble into neat patterns with the ordered domain, as observed by STM in Fig. 1a. Meanwhile, the characteristic herringbone reconstruction of the Au(1 1 1) substrate is well preserved suggesting the fairly weak molecule-substrate interaction between precursors and the Au(1 1 1) surface at RT [22,36]. Zoom-in investigation of the self-assembled structure is represented in Fig. 1b as well. Apparently, it can be identified that Br_2Py precursors are kept intact after deposition onto Au(1 1 1) at RT with the majority arranged in close-packed manner forming a brick-wall pattern. While the adsorption density is found to be around 0.89 molecule/nm^2, a rhombohedral unit cell is withdrawn and the lattice parameters are determined to be a = 11.3 ± 0.2 Å, b = 12.0 ± 0.2 Å and θ = 55 ± 2°, as highlighted in Fig. 1c. Further inspection reveals that the brick-wall-like assembly structure is mediated by delicate halogen-hydrogen bonding motifs [36], as illustrated in the proposed adsorption model in Fig. 1c. Monomers are stacked parallel while each Br substituent interacts with four adjacent hydrogen atoms and two adjacent Br atoms from neighbouring molecules, achieving a balanced bonding framework. The Br−H bonding length varies from 3.3 to 3.8 Å, which is also consistent with literature reports [43,44].

While the parallel arrangement of Br_2Py on Au(1 1 1) is found to be dominant, self-assembled monomers can also be packed in a fishbone manner, where Br_2Py is sitting exactly at the elbow site of the herringbone reconstruction of Au(1 1 1), as marked by the black square in Fig. 1b and depicted with the zoom-in view in Fig. 1c. Detailed analysis
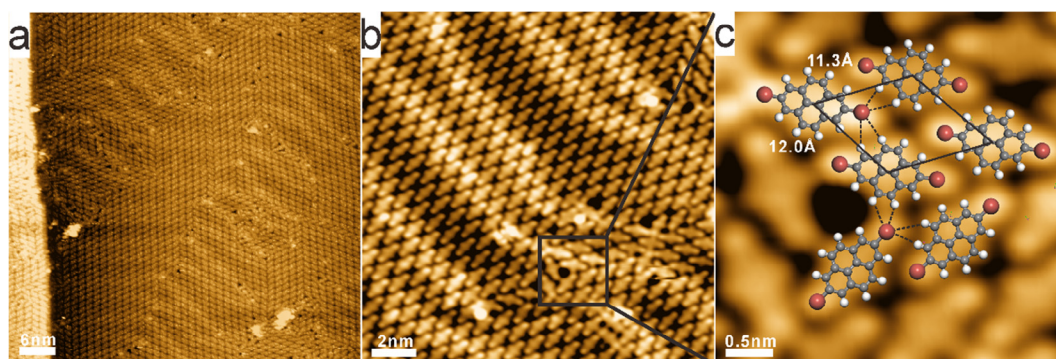
Fig. 1. Self-assembly of Br₂Py adsorbed on Au(1 1 1) at RT. (a) An overview STM image after adsorption with the herringbone reconstruction of Au(1 1 1) visible. (b) Zoom-in view with individual molecule resolved. Two packing styles of monomers are discovered: parallel and herringbone structure. (c) STM investigation with sub-molecular resolution demonstrating two molecular arrangements with the identical halogen-hydrogen bonding motif, and the DFT-optimized adsorption configuration in gas phase is overlaid on top for better illustration. Grey: carbon, white: hydrogen, brown: bromine. Scanning parameters: (a) $V_{tip} = -1.0$ V, $I = 1.0$ nA; (b) $V_{tip} = -1.8$ V, $I = 1.0$ nA; (c) $V_{tip} = -1.8$ V, $I = 1.0$ nA.

shows that the fishbone pattern is actually formed at boundaries between parallel domains, by rotating one parallel domain 60° with respect to another whilst following the threefold symmetry of the underlying Au(1 1 1) substrate.

Nevertheless, the hydrogen bonding between Br and H is still the driving force to stabilize the fishbone arrangement, and both the brick-wall and fishbone structures in fact belong to the same phase. In addition, it is worthy to point out that there exists a delicate balance between the molecule-substrate and intermolecular interaction, as the herringbone reconstruction of Au(1 1 1) is apparent after adsorption while Br₂Py precursors are orderly packed by intermolecular hydrogen bonding motifs.

As expected, dehalogenation of Br₂Py precursors on Au(1 1 1) doesn't occur at RT, which is consistent with previous reports that Au is less reactive as compared to Ag or Cu [22]. In order to initiate the dehalogenation, thermal annealing in situ was applied in sequence.

Considerable change of surface morphology is recognized after annealing to 423 K as the first step, and the STM observation is shown in Fig. 2a. Structural transformation occurs from the self-assembled arrangement of Br₂Py precursors into mixed domains with locally ordered structures. A typical close-up investigation of such multiphase nanostructures is depicted in Fig. 2b, revealing that the majority of Br₂Py precursors is kept intact whilst confined within one domain after annealing at 423 K. Moreover, these intact monomers are arranged in the same manner as the self-assembled precursors before. Interestingly, besides intact Br₂Py monomers, dimers are also found along edges between the localized domains of intact monomers, as also revealed by XPS measurements in the following. For instance, dimers are recognized with one bright spot in the middle coordinating two residues at both sides, as represented and highlighted by the coloured ellipses in Fig. 2b. Nevertheless, intermolecular bonding within self-assembly monomers should not be affected by the detached bromine atoms.
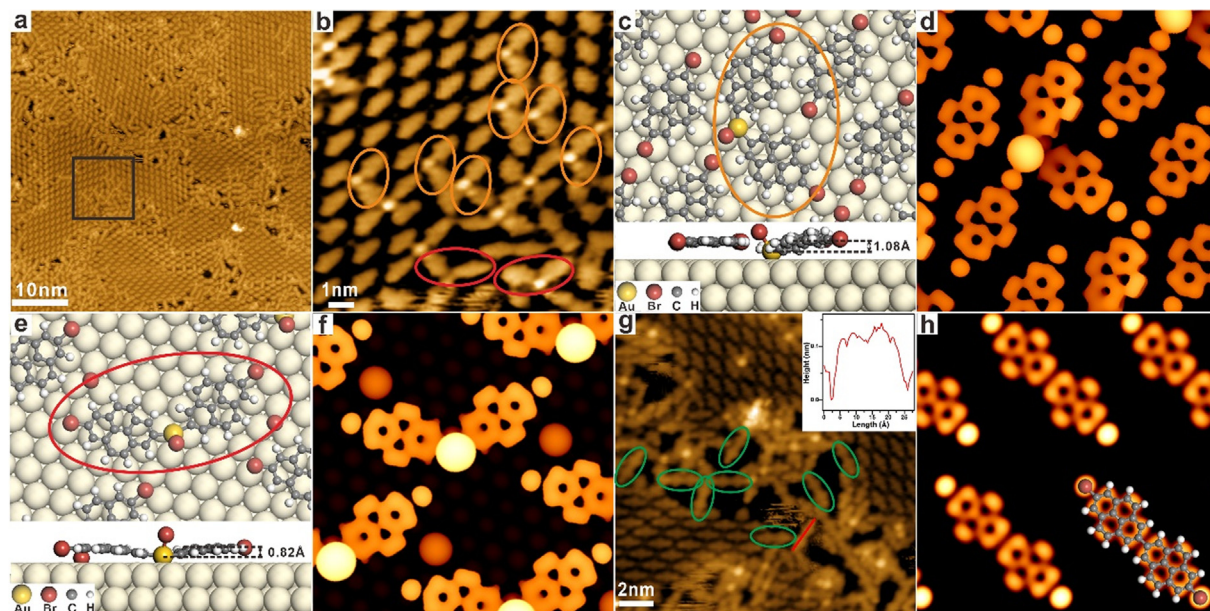
Fig. 2. The formation of OM intermediates after annealing at 423 K. (a) Large-area STM and (b) the zoom-in view of the surface topology marked with black square from panel a. As seen, OM dimers with varying shapes are formed on Au(1 1 1) after the dehalogenation of Br2Py. (c) and (e) DFT-optimized structural model of OM dimers with the corresponding simulated STM images depicted in (d) and (f). (g) Another typical STM image showing the coexistence of monomers, linear dimers and oligomers with the line profile (red) along linear dimers shown in the inset. (h) The corresponding structural model of the linear dimer predicted by DFT. Grey: carbon, white: hydrogen, brown: bromine, yellow: gold adatom. Images were taken at a) $V_{tip} = -1.0$ V and $I = 1.0$ nA; b) $V_{tip} = -1.8$ V, $I = 1.0$ nA and g) $V_{tip} = -1.0$ V, $I = 1.0$ nA. d), f), h) are simulated with the bias of -1.8 V, -1.8 V and -1.0 V, respectively. (For interpretation of the references to colour in this figure legend, the reader is referred to the web version of this article.)

Interestingly, dimers are formed with an internal angle around 90° or 120° between the two residues which might be influenced by the 3-fold symmetry of the Au(1 1 1) substrate. According to previous reports of Ullmann coupling on Au(1 1 1), the bright protrusion between residues can be assigned to the Au atom/adatom [45,46]. Therefore, it is anticipated that OM intermediates are formed in sequence of the bromine dissociation from Br$_2$Py followed by the coordinating of half-debrominated precursor to one Au atom/adatom. To further confirm such hypothesis, DFT calculations were performed with the optimized structural model illustrated in Fig. 2c and e, where dimers with the Au adatom residing in the molecular plane are revealed to be the stable configuration. Furthermore, the coordinated Au adatom is discovered to locate at the face-centred cubic or hexagonal close-packed hollow site on Au(1 1 1) as the most stable adsorption site (after a comparison of adsorption energy at different sites) coordinating the dissociated Br atom on top as well. Side-view adsorption configuration from DFT calculations shows that the Au adatom is attracted a bit closer to the substrate than the pyrene moieties with the height difference of around 0.8–1.0 Å, which is presented in Fig. 2c and e. In addition, the C–Au–C bonding angle is found to be 92° or 123° and the corresponding simulated STM images are shown in Fig. 2d and f, respectively, which seems to be reasonably consistent with experimental observations. For convincing discussion, STM simulation of OM structures adapting the surface Au atom from the first layer of Au(1 1 1) instead of the surface adatom has also been investigated for comparison and presented in Fig. S1 in the supporting information. Moreover, STM simulation of OM dimers has also been done without Br atom included atop the co-ordinated Au adatom and is illustrated in Fig. S2a in the supporting information as well. It is apparent that inconsistence with STM observations is discovered from Figs. S1 and S2a. Consequently, the bright dot sitting in between two residues observed in STM might be preferably assigned to the coordinated Au adatom with a Br atom attached on top, and this is an interesting proposal while similar demonstration has also been reported before [47,48]. On the other hand, it has also been revealed from DFT calculations that the relative binding energy of the OM dimer with one Br atom atop the Au adatom is −805.85 eV, while the OM dimer with the Br atom directly bonded to the Au(1 1 1) substrate is −805.28 eV. As the energy difference is not that big, it can be inferred that both structures are stable while the structure with Br on top of the Au adatom is more likely to occur. Further inspection of OM dimers shows that the formation of OM dimers is related to adsorption sites. For example, the Au-coordinated dimer with 120° tends to be formed at boundaries between the original brick-wall domains, while right-angled dimer also shows up around domain boundaries. Nevertheless, the halogen-hydrogen bonding between neighbouring molecules still plays a dominant role in stabilizing mixed domains comprising both halogenated monomers and OM dimers.

Interestingly, beside the formation of nonlinear dimers, annealing at 423 K also results in the formation of linear dimers and oligomers on the Au(1 1 1) surface, as marked by green ellipses in Fig. 2g. Based on the average length of these peanut-shape dimers and the absence of bright protrusion in the middle, we infer that the linear dimer is formed by reconnecting two half-debrominated molecules via the direct C–C bonding. The structural model obtained from DFT calculations is given in Fig. 2h together with the STM simulation, where the distance between adjacent residues is found to be 8.6 Å in close agreement with the STM observation. Apparently, OM dimers are constructed with the bent shape (90° or 120°), while linear dimers are also formed without Au involved, indicating the coordination effect from the Au adatom [45,46]. Nevertheless, the appearance of both Au-coordinated and non-coordinated dimers may suggest the relative stability of the OM intermediate, and obviously shows the initialization of on-surface Ullmann coupling after 423 K annealing as confirmed by XPS in the following whilst Au adatoms acting as the catalytic site.

Further annealing to 473 K leads to the formation of extended oligomers with the bamboo-like shape as presented in Fig. 3a, which

accumulate to form localized domains. Deep investigation is shown in Fig. 3b with a magnified view. Similar to the situation of OM dimers, two oligomers are anchored at a certain angle to one bright protrusion in the end which is expected to be the coordinated Au adatom, while faint bright dots are observed in the vicinity between the bamboo-shape oligomers which shall be attributed to the detached bromine atoms chemisorbed on the Au substrate [45]. Again, hydrogen bonding motifs mediate the stability of molecular chains between the bromine terminal and hydrogen atoms in peripheral from the adjacent oligomer, while the promotion of Ullmann coupling at 473 K is also supported by XPS data in the following discussion. To further understand the bonding between residues and the Au adatom, DFT optimization was performed as well. Fig. 3c shows the optimized adsorption model and the corresponding STM simulation, where reasonable consistence is observed between experimental data and calculations. Once again, such OM intermediates are predicted to host dissociated Br atoms atop the Au adatoms. For comparison, STM simulation has also been done for the OM oligomer without bromine attached on top of the coordinating Au adatom and is illustrated in Fig. S2b in the supporting information. It can be discovered that the coordinating Au appears relatively dim, which is apparently different to experimental observations. Further, more convincing demonstration can also be extracted from the comparison between experimental scans and simulations at different bias voltages, where the bright feature remains basically consistent with an additional Br atom by a series of bias-dependent STM scans and simulations. More details are shown in Fig. S3 in supporting information. Meanwhile, line profiles across the features of organometallic structures with Br atop Au at 423 K and 473 K are provided in Fig. S4 in the supporting information, which shows that bright dots are higher than organic ligands by approximately 0.8–1.0 Å and confirm the hypothesis of one Br atom on top of the Au adatom. In addition, it is found in Fig. 3b that these bright dots seem to appear more at the peripheral region as compared to the OM phase at 423 K, which is kind of interesting and might be related to the structure evolution of oligomers after annealing, as the length of molecular chains gets elongated leading into the distortion of OM structures due to space limitation. Based on DFT simulations and the above discussion, we might conclude that the Au adatom plays an important role in promoting the on-surface dehalogenation and subsequent coupling reaction.

Progressive annealing to 523 K induces the extension of bamboo-shape oligomers to as long as 10 nm with relatively high order, as shown in Fig. 3d and e, respectively. Dehalogenation of Br$_2$Py is not completed yet at this stage, since bromine terminal can still be recognized, and this is also supported by the XPS discovery afterwards. Moreover, removal of the Au adatom together with the attached bromine from OM intermediates seems to be straight forward resulting in the formation of extended 1D chains. Notably, detached bromine atoms are still clearly resolved with being well confined in between 1D bamboo-shape chains on Au(1 1 1). With the annealing temperature further increased to 573 K, 1D molecular chains are extended longer as shown in Fig. 3f, while the order of polymer chains gets declined. Meanwhile, it becomes also hard to identify bromine atoms in between polymerized chains at this stage, indicating either the partial desorption of Br adatoms from in between polymer chains or the accumulation afterwards into clusters/islands by diffusion induced by annealing at 573 K. As polymer chains are demonstrated to be stabilized by the interchain halogen-hydrogen bonding motif, decrease of the order of polymer islands shall be assigned to the desorption of bromine adatoms since the interchain bonding is reduced in the absence of Br adatoms. Another possible reason could be that the inter-chain dehydrogenative coupling starts to occur at this temperature, as one could see in Fig. 3f that most of the long chains are covalently tethered with each other at terminals and that fused wider polymer chains starts to emerge.

In order to more thoroughly investigate the mechanism of dehalogenation and coupling reaction on Au(1 1 1), XPS measurements were carried out thereafter to understand the change of chemical states
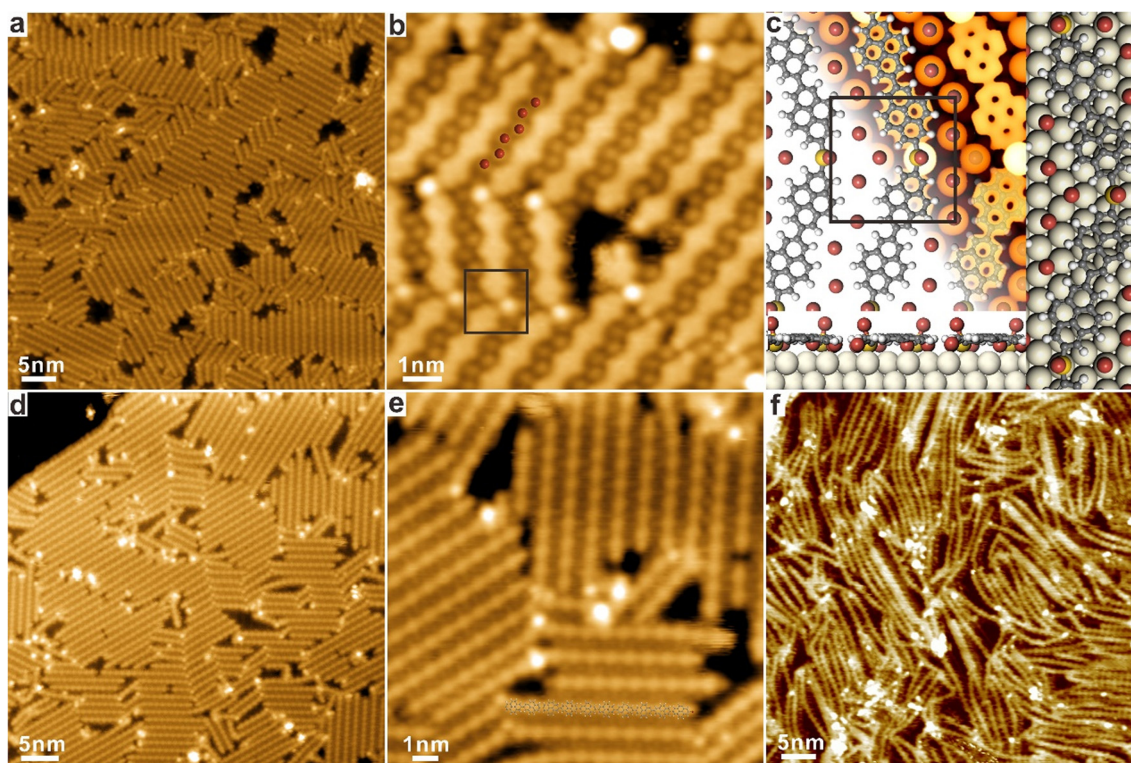
Fig. 3. A sequence of STM investigations reveals the formation of 1D bamboo-shape oligomer with increasing length after subsequent annealing. (a) Annealing to 473 K and (b) the corresponding high-resolution STM image. Adsorption model of OM oligomers proposed by DFT is illustrated in (c) with both top and side views hybridized with STM simulation, where dissociated Br atoms are either confined in between chains or chemisorbed atop Au, and the commensurability of OM chains with the Au(1 1 1) substrate can be recognized. (d) Surface topology after annealing to 523 K with elongated chains and (e) the zoom-in view. (f) Further annealing at 573 K leading to significantly extended 1D polymers. Scanning parameters: a), b), d), e) $V_{tip} = -1.0$ V, $I_t = 1.0$ nA; f) $V_{tip} = -3.0$ V, It = 0.8 nA while the bias for STM simulation in f) is -1.0 V.
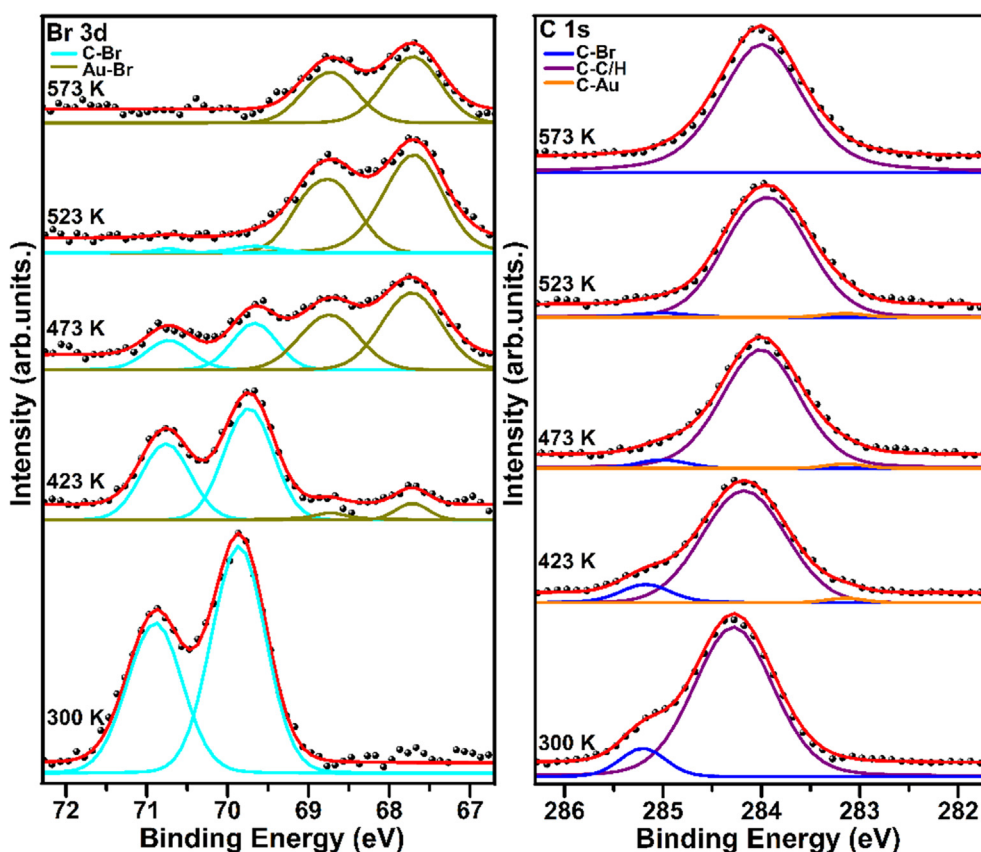
Fig. 4. Core level spectra of Br 3d and C 1s for the Br_2Py precursor adsorbed on Au (1 1 1) at RT followed by subsequent annealing to 423 K, 473 K, 523 K and 573 K respectively. Fitted components with Voigt functions are represented in solid coloured curves. Shirley background has been subtracted in the raw data for easy illustration.
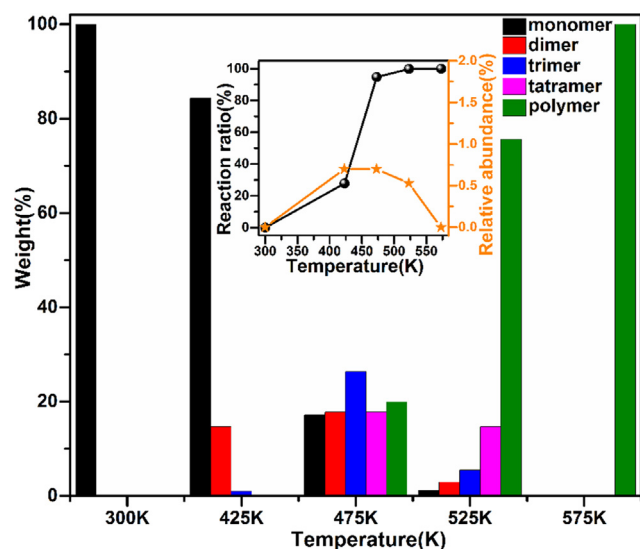
Fig. 5. Quantitative analysis of Ullmann reaction of Br_2Py on Au(1 1 1) and the length evolution of molecular chains during progressive annealing. Reaction ratio is defined as the proportion of dehalogenated precursors to the total reactant monomers, while the relative abundance of the Au−C bonding is estimated by calculating the ratio of carbon-metal bonding to C−Au linkages and C−C bonds in total as analyzed from STM images. 'polymer' stands for 5 pyrenes or more.

during reaction. High-resolution core level spectra of Br 3d and C 1s are shown in Fig. 4 from left to right, respectively, with the Shirley background subtracted for easy illustration, and the detailed fitting parameters and results are summarized in Table 1 in the supporting information, together with the raw Br 3d spectra shown as Fig. S5 for reference. Obviously, considerable changes occur in Br 3d spectra during the progressive thermal annealing. By comparison with previous reports, the spin-doublet component located at binding energy of 69.9 eV and 70.9 eV from the Br 3d spectrum at RT shall be assigned to the carbon-bonded Br atom [50], and the existence of only one spin-doublet indicates that Br_2Py molecules are intact after deposition onto Au(1 1 1) at RT, in accordance to STM observations. Similar information can also be extracted from the C 1s spectrum at RT: the peak located at 285.2 eV is ascribed to the brominated carbon atoms while the peak at 284.2 eV originates from sp^2 hybridized carbon from pyrene [51]. After annealing to 423 K, an additional doublet shows up in the Br 3d spectrum with the new Br $3d_{5/2}$ component located at 67.7 eV, and this doublet shall be attributed to the chemisorbed Br atoms on Au (1 1 1) after dissociation from precursors [10,25,47,48]. As a portion of the C−Br bonding is dissociated at 423 K, deconvolution of the C 1s spectrum is obvious. A new component located at 283.1 eV can be resolved, which is probably related to the metal- bound carbon [10,50–52]. This tiny component can therefore be assigned to the formation of C−Au bond after dehalogenation, which accounts for less than 1 percent of carbon in total as judged from peak fitting. Moreover, the intensity attenuation of the original carbon-bounded Br 3d peak also suggests the partial dehalogenation of Br_2Py at 423 K in good agreement with the intensity decline of the brominated carbon peak at 285.2 eV in the C 1s spectrum. Meanwhile, it needs to be pointed out that roughly 35% of the C−Br component is lost from the fitting analysis of C 1s spectrum at 423 K considering the desorption of Br_2Py monomers during annealing. On the other hand, less than 35% dissociated bromine is revealed to be bound to the Au substrate as indicated by the change of Br 3d spectra from RT to 423 K, suggesting the inevitable desorption of dissociated bromine after annealing.

Subsequent annealing to 473 K leads to the peak intensity being greatly enhanced of the chemisorbed Br component, which is in line with STM observations that the cleavage of C−Br bonding from

precursor becomes enormously promoted after additional annealing and dissociated Br atoms become stably adsorbed in between oligomer chains on Au(1 1 1). On the other hand, the C 1s component at 283.1 eV keeps almost constant after 473 K annealing suggesting that the population of Au-coordinated carbon remains unchanged, which is well matched to STM observations that the number of OM intermediates does not increase significantly while the length of oligomers gets apparently elongated by interconnecting more debrominated residues after annealing to 473 K. Further heating to 523 K induces a significant decline of the C−Br bonding from pristine Br_2Py precursors as reflected in both Br 3d and C 1s spectra, whereas the carbon-bonded bromine is almost gone but faintly visible at 69.7 eV/70.7 eV in the Br 3d spectrum, and similar behaviour is found for the carbon peak at 285.0 eV in the C 1s spectrum. These observations suggest that the amount of terminal bromine becomes significantly reduced and is in principle consistent with STM discovery in Fig. 3e. Meanwhile, ratio of the Au−C bonding becomes slightly weaker, which also agrees with STM measurements in Fig. 3d and e.

In the end, annealing to 573 K results in the complete disappearance of both metal-bonded and halogenated carbon components, and the only remains of the sp^2 hybridized C 1s component, as seen from the top C 1s spectrum in Fig. 4. Such behaviours indicate that Ullmann coupling dehalogenation on Au(1 1 1) is completed after annealing to 573 K. Meanwhile, the Br 3d spectrum is now represented by the single component originating from chemisorbed Br atoms, which demonstrates as well that the dehalogenation of Br_2Py precursors is completed with the retaining dissociated Br atoms chemically adsorbed on the gold substrate. Additionally, the intensity of chemisorbed Br component decreases considerably as compared to that at annealing to 473 K, revealing that chemisorbed Br atoms start to desorb from surface after 573 K annealing. This observation is consistent with the STM image in Fig. 3f that the chemisorbed Br atoms start to desorb at this stage, although bromine atoms are hard to resolve in STM due to the localized investigation capability of STM. Details of fitting parameters are summarized in Table 1 in the supporting information. Nevertheless, a downward shift of both Br 3d and C 1s spectra is observed during annealing and Ullmann coupling, which is attributed to the change of interfacial work-function caused by the chemisorbed Br atoms [52]. Meanwhile, a quantitative analysis of the Ullmann reaction ratio (defined as the proportion of dehalogenated precursors to the total reactant monomers), the relative abundance of the C−Au bonding (estimated by calculating the ratio of the carbon-metal bonding to the total amount of C−Au and C−C bonds analyzed from STM images) and the length of oligomers as a function of annealing temperature is summarized in Fig. 5 based on STM measurements, whereas a linear increase of oligomer length can be recognized and the change of relative abundance of the Au−C bonding is basically similar to that in C 1s spectra showing that the relative amount of Au−C bonding becomes almost constant (around 0.7%) from 423 K to 473 K annealing, drops at 523 K annealing and becomes zero after 573 K annealing.

To obtain an atomistic understanding of the dehalogenation mechanism of Br_2Py on Au(1 1 1) and the critical role of Au atoms/adatoms during reaction, DFT calculations combined with NEB have been carried out. To balance the computation cost and accuracy, Br_2Py is represented by a bromobenzene molecule (C_6H_5Br, as shown in Fig. 6) [20,53–55]. The initial reactant state (IS) is built as the C_6H_5Br adsorbed on Au(1 1 1) with one Au adatom nearby. It is discovered that the initial dissociation of one Br atom from one bromobenzene under the assistance of an Au adatom needs to overcome a relatively low energy barrier as compared to that assisted by an Au atom from the first surface layer (red dashed line in Fig. 6, more details can be found in Fig. S4 in the supporting information). Additionally, in order to produce an Au adatom on purpose on Au(1 1 1), an energy barrier of around 1.50 eV needs to be overcome, and additional energy of 0.85 eV is required for the adatom to diffuse to the right position, which in general can be fulfilled by the sputtering/annealing procedure during sample
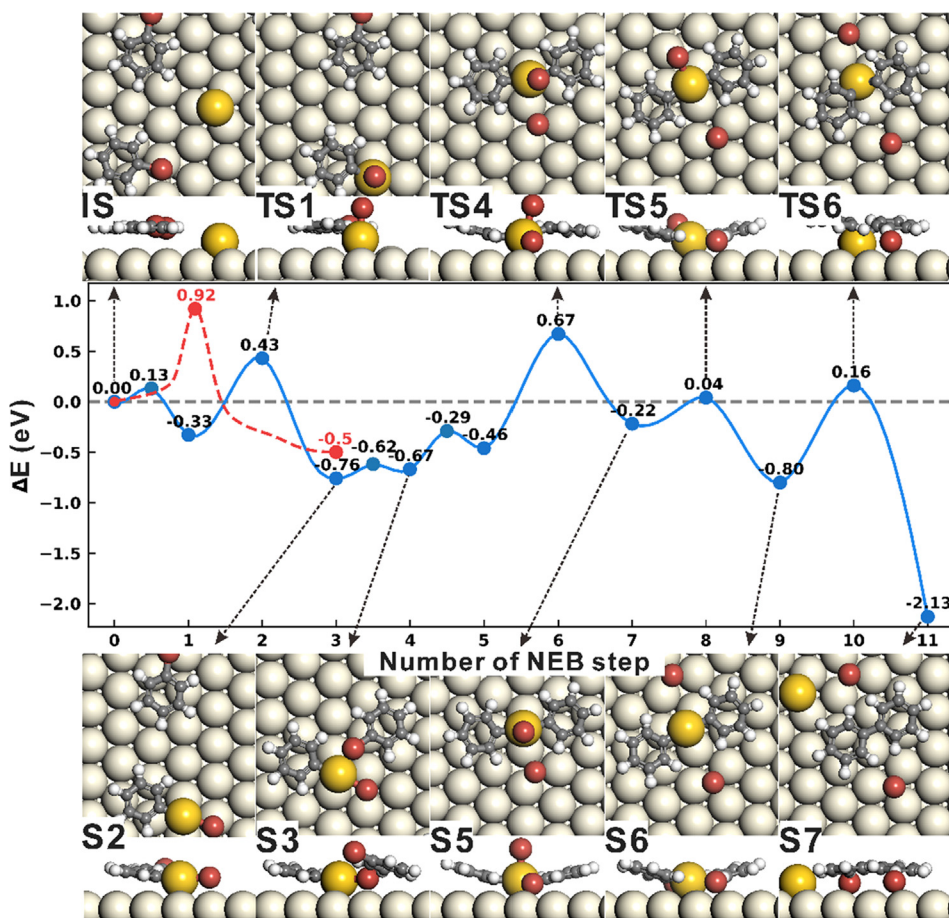
Fig. 6. Schematic diagram for the Ullman coupling reaction of bromobenzene on Au(1 1 1) illustrating the dehalogenation, followed by the formation of OM intermediate and the successive C-C coupling between dehalogenated monomers. Transitional states (TS) have also been depicted for east illustration, while adsorption models are given in both top view and side view. Red dashed line is the predicted reaction path for the dehalogenation of one bromobenzene on Au (1 1 1) excluding the Au adatom. (For interpretation of the references to colour in this figure legend, the reader is referred to the web version of this article.)

preparation. Such comparison implies that the scission of C−Br bonding seems to be quite favourable under the assistance from an Au adatom (TS1), which is subsequently followed by the formation of a relatively stable Au−C bonding with Br atop in an OM intermediate (S2). Thereafter, a second bromobenzene becomes debrominated as well via the help of the Au adatom (S3 and S4) and is bonded together to form an OM dimer whereas the Au adatom coordinates two half-dehalogenated precursors with the Au−C bonding motif and one bromine atom atop (TS4), and these reaction steps agree well to STM observations as shown in Figs. 2 and 3 [14], respectively. Subsequently, the reaction pathway from the OM intermediate with the Br−Au−C bonding (S5 and S6) to the final covalent nanostructure with direct C-C coupling (S7) needs to pass an intermediate state TS6 and overcome an energy barrier of 0.16 eV, which is slightly lower than the previous barrier of the C−Br bond scission and can be easily overcome by successive heating, in consistent with the demonstration in previous reports [26,27]. Afterwards, removing the coordinated Au adatom from the OM intermediate is convenient without breaking residues, since such reaction step is an exothermal process from TS6 to S7. After the release of Au adatom from the OM oligomer and the successive settle down of the released Au adatom nearby on surface, residues are then reconnected to form dimers with the direct C-C coupling (S7). In short, the NEB-DFT investigation reveals the Au adatom is more favoured compared to surface atoms during on-surface dehalogenation, which actively induces the formation of OM nanostructures with metal-carbon bonding.

It has been demonstrated in previous reports that the lack of Au coordinated OM chains on Au(1 1 1) can be attributed to the thermodynamic behaviour of Ullmann dehalogenation with the formation of surface-stabilized residues [28]. The observation of OM intermediates for Br_2Py precursors on Au(1 1 1) herein shall be credited to the high stability and diffusion ability of OM structures which are not anchored

by the Au(1 1 1) surface. Further, the stability of OM phases and the easy removal of Au atoms from OM structures to form covalent polypyrene chains should be close related to the Au adatom with the Br atop which stops the formation of surface-stabilized residues by coordinating dehalogenated residues, since the bromine atom can easily attract electron from Au due to its strong electronegativity which therefore makes the C−Au bonding in OM dimers and polymers distinct towards further reaction process from the situation of OM structures in the absence of Br. In addition, the OM species formed on Au(1 1 1) show a nonlinear configuration which is distinct from the linear ones formed on Ag or Cu surfaces. From the energy point of view, it is discovered that the nonlinear structure is more favourable than the linear counterpart, for instance, the nonlinear OM phase with Br atop is 0.8 eV lower in binding energy that the linear counterpart, indicating again the Br atom atop the Au adatom in OM species shall play an important role in forming the nonlinear OM configuration. Therefore, it can be proposed that Au adatoms might have interesting implications towards on-surface synthesis, for example, the realization of OM phase on Au surfaces and artificial manipulation of on-surface Ullmann reaction, besides lowering energy barrier and reaction temperature as demonstrated above. Nevertheless, as witnessed by the coexistence of nonlinear OM intermediates and linear dimers with direct C-C coupling in Fig. 2, it can also be inferred that the stability of Au coordinated OM chains during Ullmann coupling reaction might not be as robust as on other coinage metal substrates.

In the end, it needs to be pointed out that the demonstration of Au adatom assisting the Ullman coupling reaction with the formation of OM species is mainly supported by DFT and NEB calculations, while direct experimental evidence is still less clear in this work. On the other hand, the dehalogenation might also occur on terraces or defect sites, which cannot be excluded from current results. On the other hand, the

reaction pathway, intermediate species and products might also be different when the self-assembly of precursors is steered [24,25]. As judged from STM observations herein, OM dimers and oligomers are usually discovered at the boundary of the self-assembly domains, however, different OM species and products might also be observed in Ullmann coupling by tuning the self-assembly manner of Br$_2$Py on Au (1 1 1), for instance, by manipulating the arrangement of monomers from inside the domain to at the domain boundary, which will be interesting to investigate in future. It is also meaningful to address that the halogenated terminal group might have significant influence on the formation of OM intermediates. For example, OM with different nanostructures were discovered in the form of hexagonal rings or linear chains on Au(1 1 1) when alkynyl bromide group/terminal is considered in previous studies [45,46]. The difference in OM nanostructures might be assigned to the discrimination in the mobility or charge density of terminal chains among alkyls and precursors, which can be further utilized in manipulating the formation of OM nanostructures and subsequent covalent polymers on Au(1 1 1).

4. Conclusions

On-surface Ullmann coupling of 2, 7-dibromopyrene on Au(1 1 1) has been comprehensively investigated by a combination of experimental methods and first-principle calculations with STM, XPS and DFT. While the dehalogenation of Br$_2$Py on Au(1 1 1) is activated by thermal annealing at 423 K, the Ullmann coupling reaction has been further promoted by elevated annealing. Interestingly, OM intermediates with nonlinear shapes are observed on Au(1 1 1), which is expected to be induced by the partial dehalogenation of Br$_2$Py and the coordination of Au atoms between debrominated precursors. As predicted from DFT and NEB calculations, the formation of OM structures on Au(1 1 1) can be mostly assigned to the assistance from Au adatoms, which compete with the Au(1 1 1) substrate to prevent the formation of surface-stabilized residues. Progressive annealing results in further polymerization with the appearance of bamboo-shaped oligomers, and dissociated Br atoms are chemically adsorbed on top of the Au(1 1 1) substrate and confined between 1D polymerized chains, which start to desorb from Au(1 1 1) after annealing to 573 K as revealed by both STM and XPS. According to DFT with NEB calculations, Au-adatom-coordinated OM structures are favourable and extended polymerization with the direct C-C coupling is straightforward afterwards by removing Au adatoms from the kinetic energy point of view. Finally, our study might provide some valuable insights on further exploiting OM intermediates and identifying elementary reaction steps during Ullmann coupling on Au(1 1 1).

CRediT authorship contribution statement

Jinbang Hu: Conceptualization, Methodology, Writing - original draft. **Jinping Hu:** Methodology, Investigation. **Zhengde Zhang:** Software, Formal analysis. **Kongchao Shen:** Methodology, Investigation. **Zhaofeng Liang:** Data curation. **Huan Zhang:** Data curation. **Qiwei Tian:** Methodology. **Peng Wang:** Conceptualization. **Zheng Jiang:** Supervision. **Han Huang:** Conceptualization, Supervision. **Justin W. Wells:** Writing - review & editing. **Fei Song:** Funding acquisition, Project adiministration, Writing - review & editing.

Declaration of Competing Interest

The authors declare that they have no known competing financial interests or personal relationships that could have appeared to influence the work reported in this paper.

Acknowledgements

Appendix A. Supplementary material

Supplementary data to this article can be found online at https://doi.org/10.1016/j.apsusc.2020.145797.

References

[1] L. Grill, M. Dyer, Matthew, L. Lafferentz, M. Persson, M.V. Peters, S. Hecht, Nano-architectures by covalent assembly of molecular building blocks, Nat. Nanotech. 2 (2007) 687–691.

[2] J. Cai, P. Ruffieux, R. Jaafar, M. Bieri, T. Braun, S. Blankenburg, M. Muoth, A.P. Seitsonen, M. Saleh, X.L. Feng, K. Müllen, R. Fasel, Atomically precise bottom-up fabrication of graphene nanoribbons, Nature 466 (2010) 470–473.

[3] P. Ruffieux, S. Wang, B. Yang, C. Sánchez-sánchez, J. Liu, T. Dienel, L. Talirz, P. Shinde, C.A. Pignedoli, D. Passerone, T. Dumslaff, X.L. Feng, K. Müllen, R. Fasel, On-surface synthesis of graphene nanoribbons with zigzag edge topology, Nature 531 (2016) 489–492.

[4] J.P. Llinas, A. Fairbrother, G.B. Barin, W. Shi, K. Lee, S. Wu, B.Y. Choi, R. Braganza, J. Lear, N. Kau, W. Choi, C. Chen, Z. Pedramrazi, T. Dumslaff, A. Narita, X.L. Feng, K. Müllen, F. Fischer, A. Zettl, P. Ruffieux, E. Yablonovitch, M. Crommie, R. Fasel, J. Bokor, Short-channel field-effect transistors with 9-atom and 13-atom wide graphene nanoribbons, Nat. Commun. 8 (2017) 633.

[5] M. Koch, F. Ample, C. Joachim, L. Grill, Voltage-dependent conductance of a single graphene nanoribbon, Nat. Nanotech. 7 (2012) 713–717.

[6] Y.-Q. Zhang, N. Kepčija, M. Kleinschrodt, K. Diller, S. Fischer, A.C. Papageorgiou, F. Allegretti, J. Björk, S. Klyatskaya, F. Klappenberger, M. Ruben, J.V. Barth, Homo-coupling of terminal alkynes on a noble metal surface, Nat. Commun. 3 (2012) 1286.

[7] H.-Y. Gao, H. Wagner, D.Y. Zhong, J.-H. Franke, A. Studer, H. Fuchs, Glaser coupling at metal surfaces, Angew. Chem. Int. Ed 52 (2013) 4024–4028.

[8] Q. Sun, C. Zhang, Z.W. Li, H.H. Kong, Q.G. Tan, A.G. Hu, W. Xu, On-surface formation of one-dimensional polyphenylene through Bergman cyclization, J. Am. Chem. Soc. 135 (2013) 8448–8451.

[9] S. Clair, D.G. de Oteyza, Controlling a chemical coupling reaction on a surface: tools and strategies for on-surface synthesis, Chem. Rev. 119 (2019) 4717–4776.

[10] M. Lackinger, Surface-assisted Ullmann coupling, Chem. Commun. 53 (2017) 7872–7885.

[11] A. Gourdon, On-Surface Synthesis, Springer, 2016, , https://doi.org/10.1007/978-3-319-26600-8.

[12] C. Moreno, M. Vilas-Varela, B. Kretz, A. Garcia-Lekue, M.V. Costache, M. Paradinas, M. Panighel, G. Ceballos, S.O. Valenzuela, D. Peña, A. Mugarza, Bottom-up synthesis of multifunctional nanoporous graphene, Science 360 (2018) 199–203.

[13] O. Gröning, S. Wang, X. Yao, C.A. Pignedoli, G. Borin Barin, C. Daniels, A. Cupo, V. Meunier, X. Feng, A. Narita, K. Müllen, P. Ruffieux, R. Fasel, Engineering of robust topological quantum phases in graphene nanoribbons, Nature 560 (2018) 209–213.

[14] Q. Fan, J.M. Gottfried, J. Zhu, Surface-catalyzed C-C covalent coupling strategies toward the synthesis of low-dimensional carbon-based nanostructures, Acc. Chem. Res 48 (2015) 2484–2494.

[15] M.D. Giovannantonio, G. Contini, Reversibility and intermediate steps as key tools for the growth of extended ordered polymers via on-surface synthesis, J. Phys.: Condens. Matter 30 (2018) 093001.

[16] S.P. Xing, Z. Zhang, X.Y. Fei, W. Zhao, R. Zhang, T. Lin, D.L. Zhao, H.X. Ju, H. Xu, J. Fan, J.F. Zhu, Y.Q. Ma, Z.L. Shi, Selective on-surface covalent coupling based on metal-organic coordination template, Nat. Commun. 10 (2019) 70.

[17] T. Lin, X.S. Shang, J. Adisoejoso, P.N. Liu, N. Lin, Steering on-surface polymerization with metal-directed template, J. Am. Chem. Soc. 135 (2013) 3576–3582.

[18] M. Ammon, T. Sander, S. Maier, On-surface synthesis of porous carbon nanoribbons from polymer chains, J. Am. Chem. Soc. 139 (2017) 12976–12984.

[19] D. Ebeling, Q.G. Zhong, T. Schlöder, J. Tschakert, P. Henkel, S. Ahles, L.F. Chi, D. Mollenhauer, H.A. Wegner, A. Schirmeisen, Adsorption structure of mono- and diradicals on a Cu(111) surface: chemoselective dehalogenation of 4-bromo-3″-iodo-p-terphenyl, ACS Nano 13 (2019) 324–336.

[20] J. Björk, F. Hanke, S. Stafström, Mechanisms of halogen-based covalent self-assembly on metal surfaces, J. Am. Chem. Soc. 135 (2013) 5768–5775.

[21] R. Gutzler, L. Cardenas, J. Lipton-Duffin, M. El Garah, L.E. Dinca, C.E. Szakacs, C. Fu, M. Gallagher, M. Vondráček, M. Rybachuk, D.F. Perepichka, F. Rosei, Ullmann-type coupling of brominated tetrathienoanthracene on copper and silver, Nanoscale 6 (2014) 2660–2668.

[22] G. Galeotti, F. De Marchi, T. Taerum, L.V. Besteiro, M. El Garah, J. Lipton-Duffin, M. Ebrahimi, D.F. Perepichka, F. Rosei, Surface-mediated assembly, polymerization and degradation of thiophene-based monomers, Chem. Sci. 10 (2019) 5167–5175.

[23] Q. Fan, J. Dai, T. Wang, J. Kuttner, G. Hilt, J.M. Gottfried, J. Zhu, Confined synthesis of organometallic chains and macrocycles by Cu–O surface templating,

ACS Nano 10 (2016) 3747–3754.

[24] X. Zhou, C. Wang, Y. Zhang, F. Cheng, Y. He, Q. Shen, J. Shang, X. Shao, W. Ji, W. Chen, G.Q. Xu, K. Wu, Steering surface reaction dynamics with a self-assembly strategy: ullmann coupling on metal surfaces, Angew. Chem. Int. Ed. 56 (2017) 12852.

[25] Q.W. Chen, J.R. Cramer, J. Liu, X. Jin, P.L. Liao, X. Shao, K.V. Gothelf, K. Wu, Steering on-surface reactions by a self-assembly approach, Angew. Chem. Int. Ed. 56 (2017) 5026.

[26] M. Bieri, M.-T. Nguyen, O. Gröning, J. Cai, M. Treier, K. Aït-Mansour, P. Ruffieux, C.A. Pignedoli, D. Passerone, M. Kastler, K. Müllen, R. Fasel, Two-dimensional polymer formation on surfaces: insight into the roles of precursor mobility and reactivity, J. Am. Chem. Soc. 132 (2010) 16669–16676.

[27] M. Di Giovannantonio, M. Tomellini, J. Lipton-Duffin, G. Galeotti, M. Ebrahimi, A. Cossaro, A. Verdini, N. Kharche, V. Meunier, G. Vasseur, Y. Fagot-Revurat, D.F. Perepichka, F. Rosei, G. Contini, Mechanistic picture and kinetic analysis of surface-confined ullmann polymerization, J. Am. Chem. Soc. 138 (2016) 16696–16702.

[28] M. Fritton, D.A. Duncan, P.S. Deimel, A. Rastgoo-Lahrood, F. Allegretti, J.V. Barth, W.M. Heckl, J. Björk, M. Lackinger, The role of kinetics versus thermodynamics in surface-assisted ullmann coupling on gold and silver surfaces, J. Am. Chem. Soc. 141 (2019) 4824–4832.

[29] J. Eichhorn, D. Nieckarz, O. Ochs, D. Samanta, M. Schmittel, P.J. Szabelski, M. Lackinger, On-surface Ullmann coupling: the influence of kinetic reaction parameters on the morphology and quality of covalent networks, ACS Nano 8 (2014) 7880–7889.

[30] G. Galeotti, M. Di Giovannantonio, A. Cupo, S. Xing, J. Lipton-Duffin, M. Ebrahimi, G. Vasseur, B. Kierren, Y. Fagot-Revurat, D. Tristant, V. Meunier, D.F. Perepichka, F. Rosei, G. Contini, An unexpected organometallic intermediate in surface-confined Ullmann coupling, Nanoscale 11 (2019) 7682–7689.

[31] T.A. Pham, F. Song, M.T. Nguyen, Z. Li, F. Studener, M. Stöhr, Comparing Ullmann coupling on noble metal surfaces: on-surface polymerization of 1,3,6,8-tetra-bromopyrene on Cu(111) and Au(111), Chem. – Europ. J. 22 (2016) 5937–5944.

[32] A. Saywell, W. Greń, G. Franc, A. Gourdon, X. Bouju, L. Grill, Properties of benzene confined between two Au(111) surfaces using a combined density functional theory and classical molecular dynamics approach, J. Phys. Chem. C 118 (2014) 1719–1728.

[33] M.Z. Liu, M.X. Liu, L.M. She, Z. Zha, J.L. Pan, S.C. Li, T. Li, Y.Y. He, Z.Y. Cai, J.B. Wang, Y. Zheng, X.H. Qiu, D.Y. Zhong, Graphene-like nanoribbons periodically embedded with four- and eight-membered rings, Nat. Commun. 8 (2017) 14924.

[34] M. Lischka, M. Fritton, J. Eichhorn, V.S. Vyas, T. Strunskus, B.V. Lotsch, J. Björk, W.M. Heckl, M. Lackinger, On-surface polymerization of 1,6-dibromo-3,8-diiod-pyrene—a comparative study on Au(111) versus Ag(111) by STM, XPS, and NEXAFS, J. Phys. Chem. C. 122 (2018) 5967–5977.

[35] K.A. Simonov, A.V. Generalov, A.S. Vinogradov, G.I. Svirskiy, A.A. Cafolla, C. McGuinness, T. Taketsugu, A. Lyalin, N. Mårtensson, A.B. Preobrajenski, Synthesis of armchair graphene nanoribbons from the 10,10′-dibromo-9,9′-bian-thracene molecules on Ag(111): the role of organometallic intermediates, Sci. Rep. 8 (2018) 3506.

[36] T.A. Pham, F. Song, M.T. Nguyen, M. Stöhr, Self-assembly of pyrene derivatives on Au(111): substituent effects on intermolecular interactions, Chem. Commun. 50 (2014) 14089–14092.

[37] K.C. Shen, B. Narsu, G.W. Ji, H.L. Sun, J.B. Hu, Z.F. Liang, X.Y. Gao, H.Y. Li, Z.S. Li, B. Song, Z. Jiang, H. Huang, J.W. Wells, F. Song, On-surface manipulation of atom substitution between cobalt phthalocyanine and the Cu(111) substrate, RSC Adv. 7 (2017) 13827–13835.

[38] G. Kresse, J. Furthmüller, Efficient iterative schemes for ab initio total-energy calculations using a plane-wave basis set, Phys. Rev. B. 54 (1996) 11169.

[39] J.P. Perdew, K. Burke, M. Ernzerhof, Generalized gradient approximation made simple, Phys. Rev. Lett. 77 (1998) 3865–3868.

[40] S. Grimme, J. Antony, S. Ehrlich, H. Krieg, A consistent and accurate ab initio parametrization of density functional dispersion correction (DFT-D) for the 94 elements H-Pu, J. Chem. Phys 132 (2010) 154104.

[41] G. Tian, Y. Shen, B. He, Z. Yu, F. Song, Y. Lu, P. Wang, Y. Gao, H. Huang, Effects of monolayer Bi on the self-assembly of DBBA on Au(111), Surf. Sci. 665 (2017) 89–95.

[42] G. Henkelman, B.P. Uberuaga, H. Jónsson, A climbing image nudged elastic band method for finding saddle points and minimum energy paths, J. Chem. Phys. 113 (2000) 9901.

[43] W.H. Wang, X.Q. Shi, S.Y. Wang, M.A. Van Hove, N. Lin, Single-molecule resolution of an organometallic intermediate in a surface-supported Ullmann coupling reaction, J. Am. Chem. Soc. 133 (2011) 13264–13267.

[44] J.V. Barth, Molecular architectonic on metal surfaces, Annu. Rev. Phys. Chem. 58 (2007) 375–407.

[45] M. Liu, S. Li, J. Zhou, Z. Zha, J. Pan, X. Li, J. Zhang, Z. Liu, Y. Li, X. Qiu, Supramolecular self-assembly of π-conjugated hydrocarbons via 2D cooperative CH/π interaction, ACS Nano 12 (2012) 12612–12618.

[46] Q. Sun, L. Cai, H. Ma, C. Yuan, W. Xu, Dehalogenative homocoupling of terminal alkynyl bromides on Au(111): incorporation of acetylenic scaffolding into surface nanostructures, ACS Nano 10 (2016) 7023–7030.

[47] M. Di Giovannantonio, M. El Garah, J. Lipton-Duffin, V. Meunier, L. Cardenas, Y. Fagot Revurat, A. Cossaro, A. Verdini, D.F. Perepichka, F. Rosei, G. Contini, Insight into organometallic intermediate and its evolution to covalent bonding in surface-confined Ullmann polymerization, ACS Nano 7 (2013) 8190–8198.

[48] G. Galeotti, M. Di Giovannantonio, J. Lipton-Duffin, M. Ebrahimi, S. Tebi, A. Verdini, L. Floreano, Y. Fagot-Revurat, D.F. Perepichka, F. Rosei, G. Contini, The role of halogens in on-surface Ullmann polymerization, Faraday Discuss. 204 (2017) 453–469.

[50] C. Moreno, M. Panighel, M. Vilas-Varela, G. Sauthier, M. Tenorio, G. Ceballos, D. Peña, A. Mugarza, Critical role of phenyl substitution and catalytic substrate in the surface-assisted polymerization of dibromobianthracene derivatives, Chem. Mater. 31 (2019) 331–341.

[51] L. Massimi, O. Ourdjini, L. Lafferentz, M. Koch, L. Grill, E. Cavaliere, L. Gavioli, C. Cardoso, D. Prezzi, E. Molinari, A. Ferretti, C. Mariani, M.G. Betti, Surface-assisted reactions toward formation of graphene nanoribbons on Au(110) surface, J. Phys. Chem. C 119 (2015) 2427–2437.

[52] Q.T. Fan, L.M. Liu, J.Y. Dai, T. Wang, H.X. Ju, J. Zhao, J. Kuttner, G. Hilt, J.M. Gottfried, J.F. Zhu, Surface adatom mediated structural transformation in bromoarene monolayers: precursor phases in surface Ullmann reaction, ACS Nano 123 (2018) 2267–2274.

[53] Q. Li, B. Yang, J. Björk, Q.G. Zhong, H.X. Ju, J.J. Zhang, N. Cao, Z.L. Shi, H.M. Zhang, D. Ebeling, A. Schirmeisen, J.F. Zhu, L.F. Chi, Hierarchical dehy-drogenation reactions on a copper surface, J. Am. Chem. Soc. 140 (2018) 6076–6082.

[54] A. Rastgoo-Lahrood, J. Björk, M. Lischka, J. Eichhorn, S. Kloft, M. Fritton, T. Strunskus, D. Samanta, M. Schmittel, W.M. Heckl, M. Lackinger, Post-synthetic decoupling of on-surface-synthesized covalent nanostructures from Ag(111), Angew. Chem. Int. Ed. 55 (2016) 7650–7654.

[55] J. Björk, Reaction mechanisms for on-surface synthesis of covalent nanostructures, J. Phys.: Condens. Matter 28 (2016) 083002.